Chapter 10 Case Studies Illustrating the Role of Geomorphology in Assessing Volcanic Hazards

J. -C. Thouret, D. Karátson
J. C. Carracedo, V. R. Troll
G. B. M. Pedersen, M. T. Gudmundsson
R. Gertisser
J. N. Procter
S. Calvari, D. Casalbore, F. Di Traglia, A. Costa

This chapter, in relation to Chap. 9, contains five case studies from contributors who depict a range of geomorphic hazards and responses to eruptive and non-eruptive events at active volcanoes. Related to Sect. 2 of Chap. 9, the contributions are: the 2021 cone building and lava-flow eruption of Tajogaite-Cumbre Vieja, La Palma Island; the 2014–2015 Holuhraun and Bárðarbunga eruption and lava-flow field, Iceland; and the 2010–2018 PDCs and dome building at Merapi, Indonesia. Related to Sect. 3 of Chap. 9, changes induced by the 2012 Te Maari eruption, New Zealand are described, while related to Sect. 4, emphasis is on the rapid evolution of the Sciara del Fuoco at Stromboli, Italy, due to eruptions and a tsunamigenic landslide between 2012 and 2021.

1 Case Study 1

Volcanic and Geomorphic Controls on the 2021 Eruption of Tajogaite Volcano, La Palma

Juan Carlos Carracedo[1] **and Valentin R. Troll**[1,2]

[1]Instituto de Estudios Ambientales y Recursos Naturales (i-UNAT), University of Las Palmas de Gran Canaria (ULPGC), Las Palmas de Gran Canaria, Spain

[2]Department of Earth Sciences, Natural Resources and Sustainable Development (NRHU), Uppsala University, Uppsala, Sweden

© The Author(s), under exclusive license to Springer Nature Switzerland AG 2025
D. Karátson and J.-C. Thouret, *Volcano Geomorphology*, Advances in Volcanology,
https://doi.org/10.1007/978-3-031-77693-9_11

The Island of La Palma, located at the western end of the Canary Island chain, is the second youngest island in the archipelago and the one that has experienced the most historical eruptions (in the last 500 years). The most recent eruption (19 September to 13 December 2021) was located, like all the recorded historical eruptions, in the south of La Palma, on the Cumbre Vieja Ridge, and was the longest-lasting and most damaging of them all. Both the persistence of volcanism on La Palma, specifically along the Cumbre Vieja Ridge, and the considerably greater destruction caused in the most recent eruptive event, can be explained by the volcanic growth pattern of the island and by its morphology. The southbound directed volcanic activity on the Cumbre Vieja makes future volcanic activity there highly likely.

The Structure of La Palma Island

La Palma developed in three stages, corresponding to an initial cone-shaped shield volcano, the Taburiente Volcano, showing an uplifted submarine basement, and two successive southward extensions, the Cumbre Nueva and the Cumbre Vieja volcanoes. Activity has thus migrated progressively from north to south with the subaerial Taburiente shield active from about 2.1 to 0.5 Ma, initiating a southward extension from about 0.8 Ma to develop the Cumbre Nueva Ridge. This resulted in a giant westbound lateral collapse some 0.56 Ma ago, but the collapse embayment was later partially filled by the nested Bejenado Volcano. Volcanic activity then migrated further southward to form the Cumbre Vieja Ridge from about 0.45 Ma up to the present day.

Regarding the morphology, the island of La Palma thus displays successive volcanic edifices in a progressive and continuous extension towards the south, a process which persists today. This may be the result of a propagating fracture which, once initiated, continues to advance in the same direction, a fundamental process in the configuration of the island of La Palma and in the distribution of volcanism. The recent continuation of eruptive activity implies that volcanism along the Cumbre Vieja Ridge will inevitably reccur in the coming years, especially as the ridge continues on the ocean floor as an elevated raised narrow mountain range for >20 km. The eruptive centres are clustered along the ridge crest and are fed via a dense swarm of dykes, inside the ridge. These feeder dykes act as the conduits that supply successive eruptions (Fig. 1), thus increasing the anisotropy of the volcano and promoting the forceful intrusion of new dykes (Carracedo and Troll 2016, 2021).

The 2021 Tajogaite Eruption

The 2021 Tajogaite volcanic crisis started in mid September, and began with eruptions from a series of vents along a ca. 500 m long fissure on 19 September. During the three months of the eruption a major scoria cone of over 300 m in height was built up and an extensive lapilli-fall blanket and lava field was constructed (e.g. Carracedo et al. 2022). Thick lapilli deposits mantled roads and houses in the Valle de Aridane area. The almost constant lapilli airfall strongly affected the western flank of the Cumbre Vieja ridge, but also reached the airport and the island's capital Santa Cruz on the

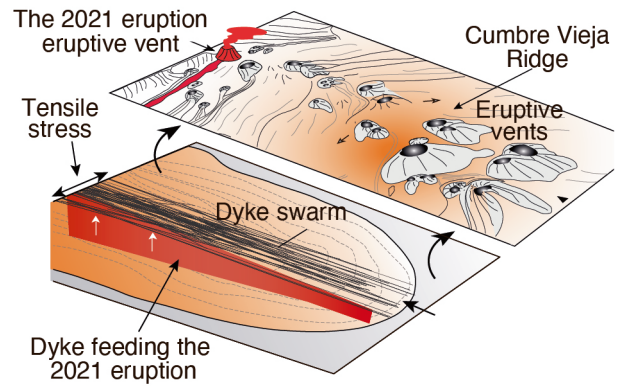

Fig. 1 The Cumbre Vieja volcanic ridge has been largely constructed within the last 125,000 years and is composed of a group of densely packed, N-S aligned cinder cones and associated lava flows. The internal structure beneath the cones is composed of a dense swarm of feeder dykes, many of which represent the conduits of past eruptions. Image modified from Carracedo and Troll (2016)

eastern side during periods when winds were blowing from the west. The lava flows had relatively high eruption temperatures (max. 1140 °C) and were consequently very fluid at times (Fig. 2), with velocities of some channelized lava flows exceeding 30 km/h (Gisbert et al.

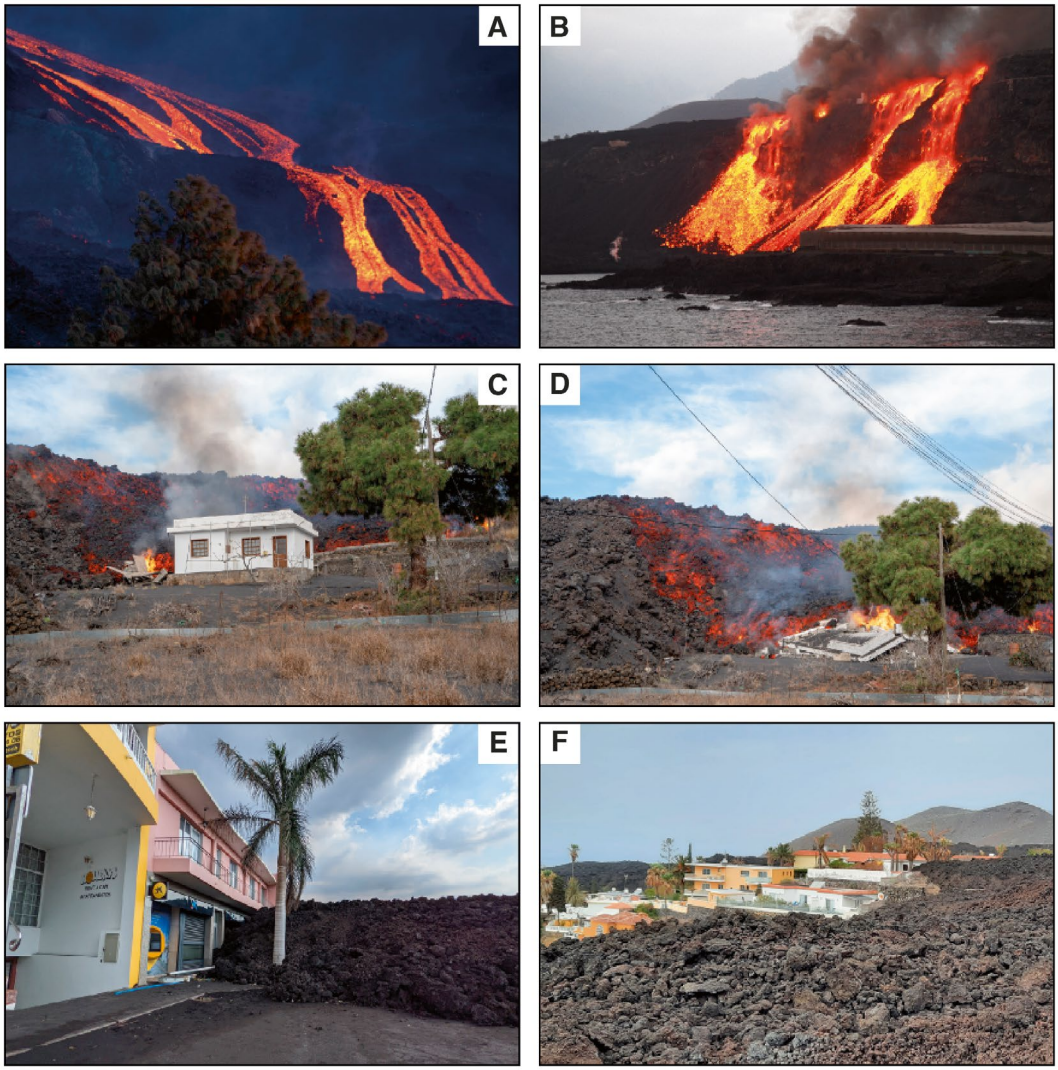

Fig. 2 Lava flows were one of the most destructive features during the 2021 La Palma eruption. **A** Rivers of lava were emitted from the central cone system and flowed downhill at 30 km/h during several episodes of the eruption, as the lava temperature commonly exceeded 1100°C near the vent (max. 1140°C). **B** These channellised (thermally insulated) lava flows allowed rapid and efficient lava transport all the way to the sea, where coastal lava platforms developed. **C, D** Frontal lava tongues and overbank facies, in turn, cooled rapidly and became blocky lava flows that advanced in caterpillar mode, slowly progressing towards buildings and destroying all man-made structures in their way, like this house in the Las Manchas area. **E** If the supply of lava at the vent ceases, lava fronts and tongues stop and freeze irrespective of topography, like here in La Laguna village, where the edge of a lava tongue entered the town. This shift to ′a′ā style emplacement, acting in a similar way to a huge bulldozer at the flow front, can sweep away everything in the path and demolish man-made structures such as houses with great ease, and contrasts with the mode of thinner lava emplacement at higher temperatures that could flow around houses, **F** As a consequence, islands of relict infrastructure (kipukas) within the main lava field are not uncommon. Photos from Carracedo et al. (2022) and Troll et al. (2024)

2023). Lava flows were one of the most destructive features during the 2021 eruption. Frontal lava tongues and overbank facies, in turn, cooled rapidly and became blocky lava flows that advanced in caterpillar mode, slowly progressing towards buildings and destroying all man-made structures in their way.

A major determining factor for the destructive nature of the 2021 eruption was the morphology of the Cumbre Vieja ridge prior to the volcanic event (Fig. 3). The ridge is triangular in shape, 1944 m high, 17 km wide in the north, and 19 km wide above sea level. In the north, the Cumbre Vieja rests on the southern edge of the Cumbre Nueva, which has collapsed and created a wide, gently sloping valley (the Aridane valley), which is densely populated and occupied by extensive plantations (e.g. Troll et al. 2024). Another densely populated area in a similar low-slope area is found on the eastern side and includes the capital, Santa Cruz de La Palma, the airport and the main harbour. The rest of Cumbre Vieja, with steeply sloping sides, is sparsely populated as there is little land suitable for cultivation. These differences in the configuration of the ridge explain why historical eruptions have had a more limited impact on infrastructure and human settlements (Fig. 3). The 2021 eruption of the Tajogaite volcano changed this pattern which may be a key

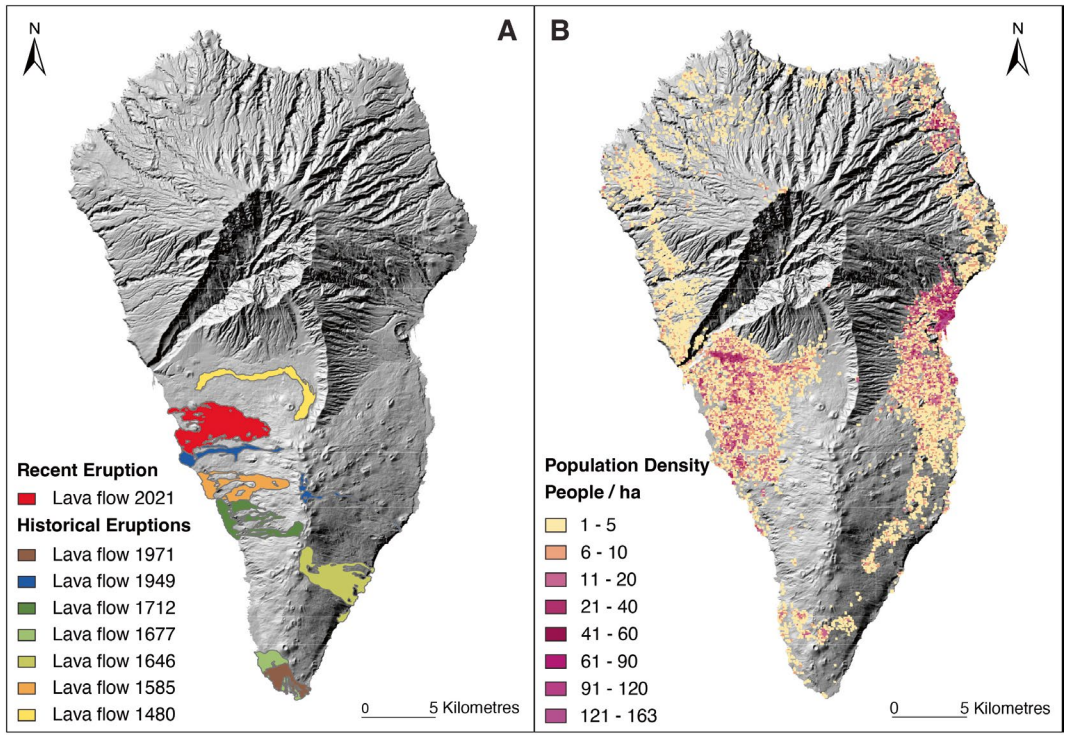

Fig. 3 **A** Slope map of the Cumbre Vieja ridge with historical eruptions outlined in colour. Past eruptions located in the southern part of the Cumbre Vieja caused no casualties and little damage to settlements and infrastructure. **B** In contrast, the eruption of the Tajogaite Volcano in 2021 was considerably more destructive, as it was located in the much flatter upper third of Cumbre Vieja, which is more densely populated and contains extensive banana plantations. From Troll et al. (2024). The eruption destroyed over 2900 buildings, devastated some 12 km^2 of farmland and settlements through lava flows and thick lapilli cover, destroyed over 90 km of vital roads, and led to the evacuation of almost 8000 people (e.g. Carracedo et al. 2022), with a total estimated cost of damage between 900 million and 1 billion euros. Since future eruptions along the Cumbre Vieja are almost inevitable, it is imperative that action is taken to ensure the safety of the island's growing population from similar future events

reason for many people having underestimated the potentially devastating effects of eruptions on the island.

For these reasons, it is likely that future eruptions will occur again on La Palma, most probably on the Cumbre Vieja ridge, with the expected damage depending primarily on the location of the eruptive centres and the consequent lava flow routes. The devastation caused by the eruption in 2021 was not a result of eruption magnitude, which was only marginally larger than other historical events, but because of the increasing vulnerability due to population growth and increasing rural land use on the lower slopes of the volcanically active Cumbre Vieja Ridge (Fig. 3).

2 Case Study 2

Holuhraun Eruption 2014–15: Lessons Learned from the Development of a Large Lava Flow Field in Iceland

Gro Birkefeldt Moller Pedersen[1] **and Magnús Tumi Gudmundsson**[1]

[1]Nordic Volcanological Center, Institute of Earth Sciences, University of Iceland, Sturlugata 7, 102 Reykjavík, Iceland

The 2014–2015 eruption at Holuhraun in the Bárðarbunga-Veiðivötn volcanic system was the largest eruption in Iceland since the 1783–1784 AD/CE Laki eruption. The lava field has an area of 84 km^2, an estimated bulk volume of 1.44 $km^3 \pm 0.07$ and the mean output rate over the six months was ~90 m^3/s (Gudmundsson et al. 2016; Pedersen et al. 2017). Bárðarbunga central volcano, located in the northwest corner of the large Vatnajökull ice cap, is covered by up to 800 m of ice within its 11 by 8 km wide caldera (Björnsson and Einarsson 1990). The associated fissure swarm is mostly subaerial and lies on the boundary between the North American and Eurasian plates, extending 80 km to the southwest and 80–125 km to the north (Hjartardóttir et al. 2016).

An intense seismic swarm began at Bárðarbunga on 16 August 2014. Over the following 11 days the formation of a 48 km-long segmented dyke could be tracked by observations of seismicity and deformation (Sigmundsson et al. 2015). A sequence of large earthquakes (M4-M5.8) started on 20 August and marked the start of a gradual caldera collapse (Gudmundsson et al. 2016). A few ice cauldrons developed in the glacier above the dyke path suggesting minor subglacial eruptions (Sigmundsson et al. 2015). The dyke terminated at a shallowly-dipping floodplain, 8 km north of Vatnajökull. On 29 August a minor, 4-h long, eruption took place along a 600 m fissure and on 31 August the volcanic fissure was re-activated, reaching 1.8 km in length, marking the onset of the 6-month-long effusive eruption, which ended on 27 February 2015. Minor effusive eruption was observed on 5–6 September 2 km south of the main fissure (Pedersen et al. 2017).

The first phase of the eruption (31 August to mid-October) was typified by channelized lava flows, 1–2 km in width and up to 17 km in length (Pedersen et al. 2017). In the first few days slabby pāhoehoe sheet flows (flow velocities of 800–1000 m/h) changed into rubbly pāhoehoe and then into a'ā downstream. Subsequently short-lived morphological changes from a'ā lava to rubbly pāhoehoe to a'ā were observed multiple times at the active flow front (flow velocities up to 65 m/h). During this phase the 1.8 km fissure partly closed down and activity became concentrated into an ~500 m-long elongated crater with a lava lake, which fed the rest of the eruption. A 1 km^2 lava pond ~1 km east of the vent formed in the second phase of the eruption (mid-October to end of November) that controlled the emplacement of subsequent flows, which slowed down and shortened in length over time (to ~5 km). By the end of November inflation plateaus developed in the lava channels that were active in September 2014 (Pedersen et al. 2017). These were surface manifestations of a growing lava tube system, which became the dominant lava transport system in the third phase (December to end-February 2015). These tubes fed breakouts of

primarily spiny pāhoehoe (flow velocities of 1–4 m/h) that resurfaced >19 km^2 of lava and extended the entire length of the flow field. Thus the lava field changed from horizontal expansion, to growth, primarily by inflation, and vertical stacking of lobes (Pedersen et al. 2017).

The 2014–15 Holuhraun lava is classified as olivine tholeiite and the composition was remarkably uniform throughout the eruption (Halldorsson et al. 2018), consistent with an eruption fed from a homogenized magma chamber beneath the Bárðarbunga central volcano. There, a downsag-type caldera subsidence was observed reaching a maximum of 65 m in the centre (Gudmundsson et al. 2016). The uniform composition and the shallow dipping substrate suggest that morphological changes in the lava were caused by variations in flow velocity and local flux influencing crust formation (Pedersen et al. 2017).

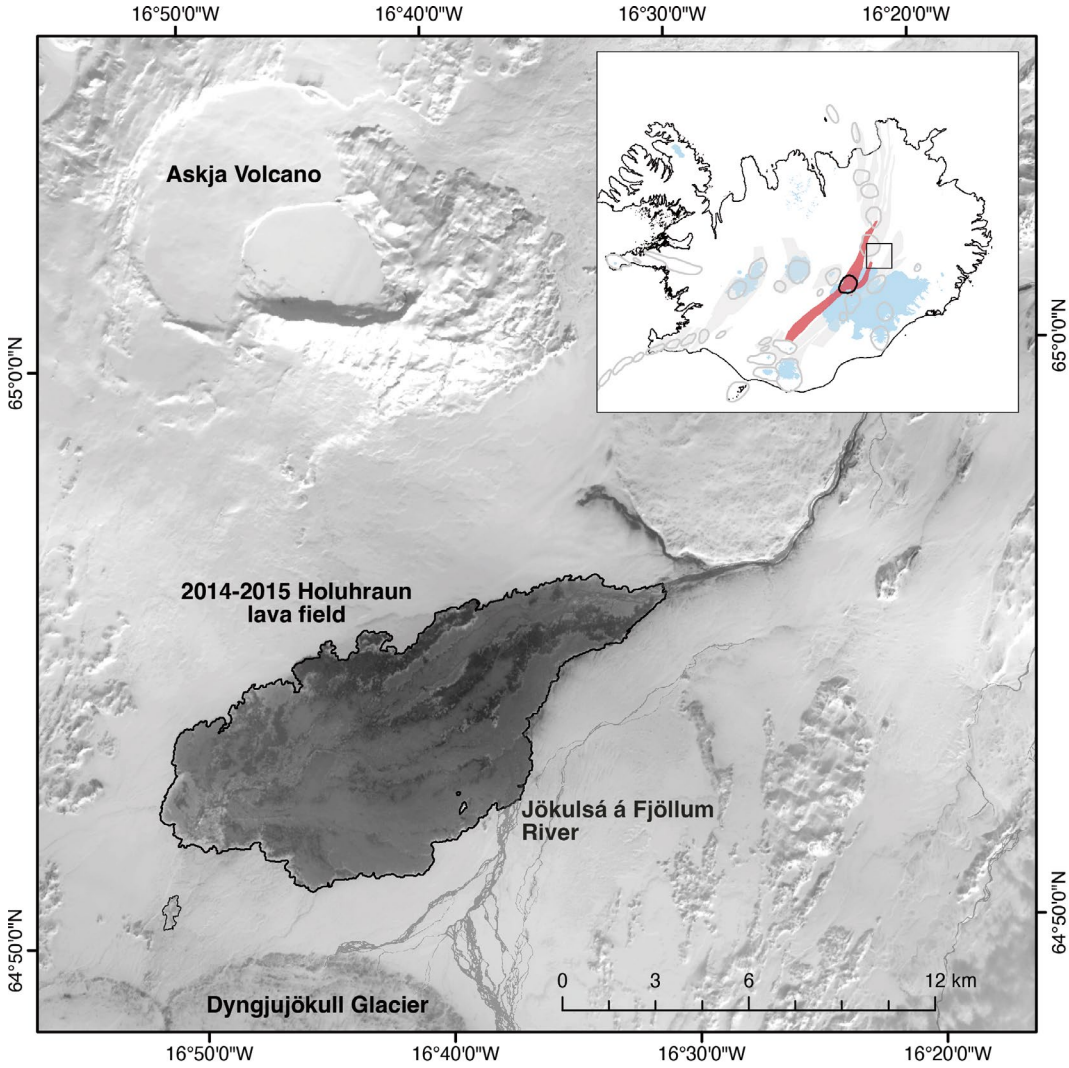

Fig. 1 The new Holuhraun lava field imaged by a LANDSAT on 2 April 2015, 33 days after the eruption stopped. The location of Holuhraun is marked by the black box on the inset map of Iceland in the upper right corner. The glaciers are shown in blue and the Icelandic volcanic systems are marked in grey. The fissure swarm of the Bárðarbunga-Veiðivötn volcanic system is highlighted in red and its central volcano is marked with a black circle

Fig. 2 First day of the Holuhraun eruption, with a near-continous fire curtain along the 1.8 km-long fissure (31 August 2015; Photo by Gro B. M. Pedersen)

At the beginning of this volcanic event the main concern was the potential danger of the eruption migrating southwards, under the Vatnajökull ice cap, causing ice melting and subsequent flooding coupled with tephra fallout. However, this did not happen. Instead, the main hazard turned out to be the release of volcanic gases with a total SO_2 emission of ca. 9.6 Mt. (Barsotti et al. 2022). Gas impacted air quality, with SO_2 concentration exceeding 1000 µg/m^3 in several instances, causing a need for increase in health care visits and treatment for asthma in Iceland. In Europe, the hourly air quality standard of 350 µg/m^3 was also exceeded in a few places in September 2014 (Barsotti et al. 2022) (Figs. 1 and 2).

3 Case Study 3

The Large-Magnitude 2010 Eruption and Post-2010 Activity of Merapi Volcano, Indonesia

Ralf Gertisser[1]

[1]School of Geography, Geology and the Environment, Keele University, Keele, ST5 5BG, UK

Rising almost 3000 m above the city of Yogyakarta in Central Java, Indonesia, Merapi volcano is renowned for its almost continuous eruptive activity and frequent occurrence of hazardous pyroclastic density currents (PDCs).

Most eruptions in the 20th and early twenty-first century followed Merapi's usual pattern of prolonged lava dome growth and subsequent gravitational dome failure to produce PDCs that mostly affected the W, SW and S slopes of the volcano, up to 10 km from the summit. The most significant recent eruption of this type occurred in 2006, when PDCs flowed down the SW and S flanks, causing destruction and fatalities in the village of Kaliadem on the bank of the Gendol River (Kali Gendol) valley (Gertisser et al. 2023).

The 2010 Eruption of Merapi and Its Environmental Effects

When Merapi erupted again in 2010, it produced the volcano's largest eruption since 1872, characterised by a Volcano Explosivity Index of 4, and the deadliest eruptive event since 1930. Moreover, the style of the 2010 eruption differed markedly from previous eruptive events (Gertisser et al. 2023). Most notably, the eruption began with partially laterally directed explosions on 26 October, producing PDCs channelled into Kali Gendol and toward the village of Kinahrejo (Fig. 1a). A lava dome formed only a few days after the initial explosions, with unprecedented growth rates of 25 m^3 s^{-1} and frequent explosive and gravitational dome failures that produced PDCs channelled mainly into Kali Gendol. During the climactic eruption phase on 5 November, a series of explosions rapidly destroyed this dome and produced a large summit crater and its downslope extension—the Gendol breach—both open to the SE (Fig. 1b). Dilute, high-energy (blast-like) PDCs were generated at the peak of the eruption and concomitant dense, valley-confined PDCs, of which at least one travelled about 16 km along Kali Gendol, caused widespread devastation on Merapi's south flank and about 400 casualties (Fig. 1c). In a later phase on 5 November, PDCs rich in pumice and scoria formed, followed by renewed dome extrusion at a rate exceeding the already high rates of the pre-climax dome extrusion phase. The eruption intensity declined on 8 November, but lahars, which had already started during the eruption, continued for several years, sweeping down all major valleys, and causing considerable environmental impact. Lahar runouts exceeded 15 km and even reached Yogyakarta on some occasions, destroying Sabo dams and bridges, affecting the road network, and destroying more than 800 houses. As a result of the eruption, many areas that were affected by PDCs have remained uninhabitable, and nearly 400,000 people were displaced from their homes and accommodated in temporary or permanent residences.

Post-2010 Activity of Merapi

After the 2010 events, volcanic activity at Merapi continued (Gertisser et al. 2023; Global Volcanism Program 2023). Following a gradual return to background levels, the background activity was interrupted by a period of phreatic explosions from 2012 to 2014, and again in 2018. A common feature of these short-lived eruptions was the lack of obvious early warning signs, making such activity difficult to forecast. A Vulcanian explosion on 1 June 2018 signalled the beginning of a new magmatic episode, with a new lava dome appearing at the summit on 11 August 2018, marking a return to typical 'Merapi-type' activity following the 2010 eruption. The new dome piled up on top of the 2010 lava dome and grew intermittently and at a relatively low rate. The activity increased

Fig. 1 **A** ASTER false-colour satellite image from 15 November 2010, showing pyroclastic density current (PDC) and minor lahar deposits of the 2010 eruption of Merapi filling the valleys of Kali Gendol, Kali Opak and Kali Woro on Merapi's S flank (light grey). The dark grey area north of the Merapi Golf course was affected by dilute PDCs, causing almost total devastation. — Source: NASA Earth Observatory (Digital Global, November 2010). (**B, C**) Impacts of the 2010 eruption: **B** Summit crater, open to the SE, formed during the 2010 eruption, with its downslope extension, the Gendol breach. **C**. House in Kinahrejo, destroyed during the climactic eruption phase on 5 November 2010. **D** UAV image from 16 September 2021, showing two simultaneously growing, active lava domes at the summit of Merapi: the SW dome and the central dome (after Gertisser et al. 2023) ▶

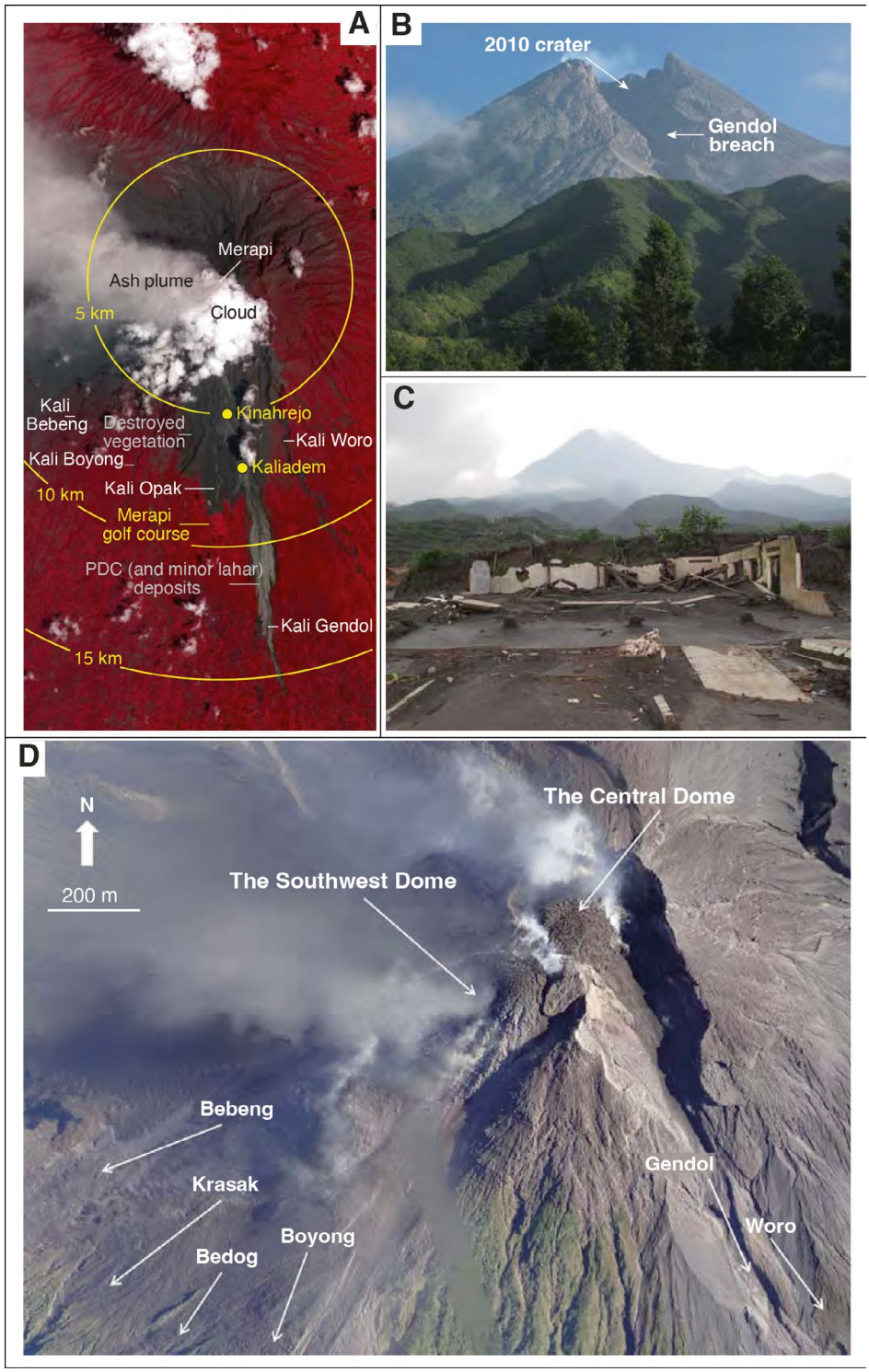
A
Merapi
Ash plume
5 km
Cloud
Kali Bebeng
Destroyed vegetation
Kinahrejo
Kali Woro
Kali Boyong
Kaliadem
10 km
Kali Opak
Merapi golf course
PDC (and minor lahar) deposits
Kali Gendol
15 km
B
2010 crater
Gendol breach
C
D
N
200 m
The Central Dome
The Southwest Dome
Bebeng
Krasak
Bedog
Boyong
Gendol
Woro

in September 2019, causing several explosive eruptions in the months to follow. During November and December 2020, the deformation rate continued to accelerate, and numerous rock avalanches were reported. Incandescence at the summit on 31 December 2020 hinted at the arrival of new magma at the surface, and on 7 January 2021, the appearance of a new dome in the SW part the summit just below the SW rim (SW lava dome) was reported. Several PDCs, accompanied by a significant explosion with an ash column of 12 km altitude and ash fall in the areas surrounding Merapi, occurred on 27 January 2021. On 17 February 2021, two domes were noted in the summit area, the SW lava dome, and a new dome in the centre of the 2010 summit crater (central lava dome). This has led to the remarkable situation of two simultaneously growing, spatially separate active lava domes at the summit of Merapi (Fig. 1d).

Both domes continued to grow in the following months, accompanied by incandescent rock avalanches and short-runout PDCs up to 2–3 km from the summit in the S and SW sector, particularly from the SW lava dome, but occasionally also down Kali Gendol due to failure of the central lava dome. By early 2022, both the SW lava dome and the central lava dome reached their maximum volume of 1.67 million m^3 and 3.23 million m^3, respectively. Since then, magma extrusion, dome growth and partial dome destruction by rock falls, rock avalanches, small PDCs, and explosions, particularly from the SW lava dome, have continued at high levels. Rock avalanches and small PDCs derived from the SW lava dome typically travel no more than 2 km in the SW and S sector, reaching the upper parts of the Bebeng and Boyong drainages. Geomorphic changes at Merapi's summit have typically been minor during this period due to continuing lava effusion and dome growth, balanced by concurrent partial dome collapse. More significant geomorphic changes have occurred only during either a period of dome growth or a period of dome failure. In December 2023, due to the continuing high-level of activity, the volcanic alert level at Merapi was still at level 3 (on a scale of 1–4), and the population was advised, depending on their location, to stay clear of areas between 3–7 km from the summit (Global Volcanism Program 2023).

4 Case Study 4

Mt. Tongariro, New Zealand: Geomorphic Changes Associated with the Te Maari Eruption of 6 August 2012

Jonathan N. Procter [1]

[1]Volcanic Risk Solutions, School of Agriculture and Environment, Massey University, Palmerston North, New Zealand

Mt. Tongariro, New Zealand is situated within the Taupo Volcanic Zone. The edifice has been constructed over the last 500 ka through the formation of different volcanic centres that are nested within a complex graben structure. Each centre has a history of discrete explosive and effusive periods related to the formation and construction of volcanic craters or cones (Hobden 1997). The Tongariro complex is deeply eroded in places, with numerous glaciogeomorphic features. Glacial retreat contributed to the generation of lahars by freeing up available water and exposing loose unconsolidated material in valleys and the massif slopes. The depositional sequences of laharic activity described in distal areas are sedimentologically and texturally different to debris flow and volcanic induced landslides preserved on more active proximal areas of the volcano. Lahars (including hyperconcentrated flows and debris flows) and debris avalanches are not commonly associated with this volcanic complex. Where they do occur in the stratigraphic record, they are a result of secondary processes of remobilisation of material or weathering/erosion of a stable edifice/cone rather than associated with explosive activity or vent formation.

The Te Maari Craters were most likely formed from activity that started at around 14 ka following the last glacial maximum. The area consists of an upper crater and an older lower crater, with the upper crater being more active historically. The 6 August 2012 eruption of the upper Te Maari Crater and the formation of new vents were similar to past eruptive episodes (1892, 1896; Hobden 1997). Small phreatic eruptions like the one that occurred on 6 August 2012 are relatively less hazardous than other phenomena in the Tongariro Volcanic Centre due to hazards from hydrothermal/phreatic eruptions being more localised (with deposits being <1 km radius). The 6 August Upper Te Maari eruption was a short-lived phreatic eruption that produced an eruption column between 6 and 10 km in height. There were distinctive events associated with the 6 August eruption; a small flank collapse that resulted in a debris flow, excavation and formation of vents and blasts/surges, ejection of ballistics and the phreatic eruption which distributed ash. Hill (1893) highlighted related eruption products such as surges (or pyroclastic flows) and debris flows (or lahars) associated with past eruptions.

Siebert et al. (1987) classifies the production of mass flows caused by collapse into two categories: those that are magmatic, which have syn-eruptive directed blast deposits (Bezymianny type), and those that are solely phreatic eruptions, commonly with debris avalanches associated with the onset of the eruptive activity (Bandai-type). Regarding the Bandai eruption of 1888, Yamamoto et al. (1999) suggested that the precursory seismic activity and the collapse of the volcanic edifice released the hydrothermal system, producing a debris avalanche and pyroclastic flow. The 6 August sequence of events could be classified as a Bandai-type.

The 6 August 2012 eruption produced measurable geomorphic changes (Fig. 1). LiDAR and aerial photos were collected after the event and compared to pre-existing aerial and elevation data (10 m, contour derived digital elevation models from topographic maps). Digital elevation model (DEM) analysis of the change (Procter et al. 2010) of the Upper Te Maari Crater (280,000 m^3) identified a new vent (200,000 m^3) and fissures (148,000 m^3) as well as a significant wedge of material (683,000 m^3) that slipped from the western flank of the crater that can be attributed to the source of a debris flow that propagated 2 km from source. The debris-flow deposit, from its morphology, can be subdivided into two sections: an upper (700 m long) segment and a lower segment, with the lower segment being further divided into three sections representing individual flow pulses that show a pattern of erosion on steep channels and deposition on flatter areas. The individual pulses of the flow (~1 min for each pulse) entrained material (up to 50% and 100% of their original volume) to runout up to 2 km from the source. The dynamics of the flow involved a change in elevation of 202 m and a runout (planar) of 769 m, indicating an H/L ratio of 0.26, consistent with the mean mobility of other cold rock, debris flows/avalanches. The area/volume ratio 0.125 indicates a flow similar to other debris flows (at the lower end of the lahar spectrum) where its runout is controlled by frictional regimes.

Velocities calculated from super-elevations indicate a pattern of pulses of material accelerating (down steep slopes) up to 11 ms^{-1} away from depositional areas and decelerating (9–10 ms^{-1}) on depositional, flatter areas. The initial stages of the debris flow or collapsing mass indicate higher velocities of 15 ms^{-1}. The average accelerations calculated would indicate a value of 11.5 $m.s^{-1}$ and an emplacement time of 215 s (3.5 min). Jolly et al. (2014a) highlight in seismic records that a lower frequency, low amplitude signal was recorded for approximately 4 min before the actual eruption at 11.52 UTC. If ~11:49 UTC marks the failure of the upper scarp and onset of the debris avalanche, and 11:51:50 marks the time that the debris flow entered the lower channel, then the debris avalanche would have propagated at approximately 18 m/s. This propagation time is consistent with the average calculated velocity of 11.5 ms^{-1} and an emplacement time of 215 s (3.5 min).

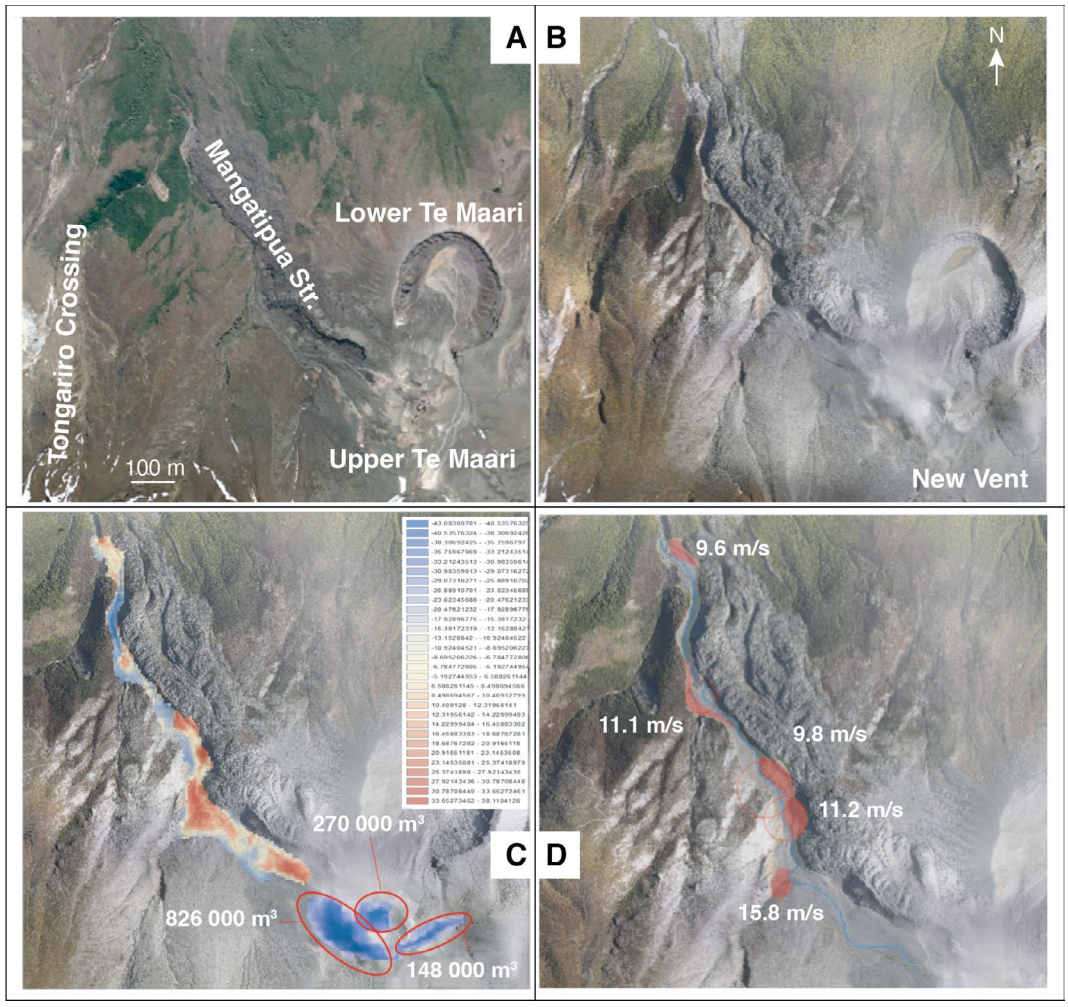

Fig. 1 Te Maari Craters and the Mangatipua stream. **A** 2004 orthophoto, pre-event. **B** 2012 orthophoto, post-event. **C** DEM difference map showing areas of volumetric change and volumes associated with the creation of new vents. **D** Velocities associated with superelevation of pulses within the flow

Using the volume displaced from the source area and the density of the material from hydraulic conductivity measurements, combined with the area of the displaced mass, we can calculate that a lithostatic pressure applied by that mass would be equivalent to 0.5 Mpa. Questions remain as to whether the release of this pressure and mass capping the area, retarding the heating and expanding the hydrothermal system could be enough to trigger the eruption. This process of collapse along weakened structures of the edifice of a cone is a commonly recognised trigger for debris avalanches, and while this process modifies the geomorphology of the edifice, it can also alter volcanic processes inducing the rise of magma and eruptions (e.g. Zemeny et al. 2023).

Jolly et al. (2014b) highlights the importance of undertaking geomorphological assessments prior to and after the eruption. Quantifying the geomorphic impact is an important contributor for assessing hazard impact, and can also be incorporated into models and mitigation strategies for future risk management.

5 Case Study 5

Rapid Geomorphic Evolution of the Sciara del Fuoco, Stromboli

Sonia Calvari[1], Daniele Casalbore[2], Federico Di Traglia[3], Antonio Costa[4]

[1]Istituto Nazionale di Geofisica e Vulcanologia, Osservatorio Etneo—Sezione di Catania

[2]Dipartimento di Scienze della Terra, Università degli Studi di Roma "La Sapienza"

[3]Istituto Nazionale di Geofisica e Vulcanologia, Osservatorio Vesuviano—Sezione di Napoli

[4]Istituto Nazionale di Geofisica e Vulcanologia, Sezione di Bologna

Stromboli volcano, famous worldwide for its mild and persistent Strombolian explosive eruptions, is an active volcanic island in the Mediterranean Sea. It also has occasional effusive eruptions (Calvari and Nunnari 2023), as well as rapid landscape build up and erosion (Di Traglia et al. 2022), summit crater failures (Di Traglia et al. 2018), flank collapses (Di Traglia et al. 2023), and tsunamigenic landslides (Chiocci et al. 2008). Effusive eruptions span in volume from a few tens to a few millions of m^3 (Calvari et al. 2005; Di Traglia et al. 2018), and can just accumulate within the crater depression (Calvari and Nunnari 2023), or spread along the barren upper Sciara del Fuoco slope. More rarely, long-lasting flank eruptions involve the opening of eruptive fissures along the flanks of the volcano (Calvari et al. 2005), leading to the creation of new land and coastal modifications and its gradual erosion (Casalbore et al. 2021).

To assess the rapid geomorphic phenomena taking place within the Sciara del Fuoco, the steep and unstable northwestern submarine-subaerial slope of the volcano, we looked at multi-platform and multi-temporal topo-bathymetric surveys, along with remote sensing data, from the past decade. This dataset encompasses a variety of topographic data sources, including multi-temporal digital elevation models (DEMs) generated through Light Detection and Ranging (LiDAR) technology and photogrammetry, utilizing images acquired from PLÉIADES satellites and Unmanned Aerial Vehicles (UAVs) (Di Traglia et al. 2022). In addition, high-spatial-resolution (HSR) optical imagery from QUICKBIRD and PLÉIADES satellites, as well as COSMO-SkyMed Synthetic Aperture Radar backscattering images, have been used to detect topographic changes (Casalbore et al. 2021). Offshore data was collected using repeated multibeam bathymetric surveys (MBES) and Side Scan Sonar (SSS) backscatter mosaics of the submarine flank (Di Traglia et al. 2022). The measurements were validated through direct observations of eruptive activity and geomorphic processes using monitoring webcams and repeated field inspections conducted over the time period (Calvari et al. 2005).

Based on the available geological data, the Sciara del Fuoco was formed through a lateral collapse event approximately 5.5 ka. Subsequently, significant landslides, accompanied by tsunami events, occurred during the Middle Ages (around 1 ka), and on 30 December 2002 (Casalbore et al. 2020 and reference therein). This latter event was triggered by the intrusion of magma into the Sciara del Fuoco, which coincided with the onset of the 2002–2003 flank eruption (Di Traglia et al. 2023). The landslide that caused the tsunami waves that struck the northern coast of the island involved a complex movement, characterised by the displacement of some 100–300 million m^3 of material, which varied between different stages of the landslide. Of this volume, only 21.1 million m^3 of material collapsed, of which approximately 9.5 million m^3 were mobilised in the submarine zone and 11.6 million m^3 were re-deposited between the coastal and submarine zones (Casalbore et al. 2020; Di Traglia et al. 2023).

Following the 30 December 2002 landslide, Stromboli experienced phases of significant material accumulation in the Sciara del Fuoco,

primarily linked to flank eruptions (2007, 2014, 2019), as well as periods of increased eruptive activity characterized by frequent explosions, lava overflows from the crater, and collapses of the crater rim (e.g. 2012–13, 2021, 2022).

The integrated analysis of this large dataset revealed that fluctuations in 'typical' volcanic activity led to the gradual accumulation of erupted material on the Sciara del Fuoco slope during periods of increased explosion frequency. Conversely, during periods of reduced explosion frequency, the dominant processes observed were subaerial weathering and marine-driven reworking. 'Anomalously intense' eruptive phases, characterized by the emission of lava flows and/or high-intensity explosive activity resulting in pyroclastic density currents (PDCs), rapidly led to significant accumulation and erosion of the Sciara del Fuoco slope, mainly down to a depth of 300 m underwater. This dynamic has two main implications: (i) the alternation of brecciated lava and heterogeneous volcaniclastic deposits, often lacking lateral continuity, may influence the stability of the Sciara del Fuoco slope (Di Traglia et al. 2023); (ii) lava flows or PDCs entering the sea possess the potential for seafloor erosion and/or failure (Casalbore et al. 2020), which has implications for modeling both PDCs and tsunami generation (Figs. 1, 2 and 3).

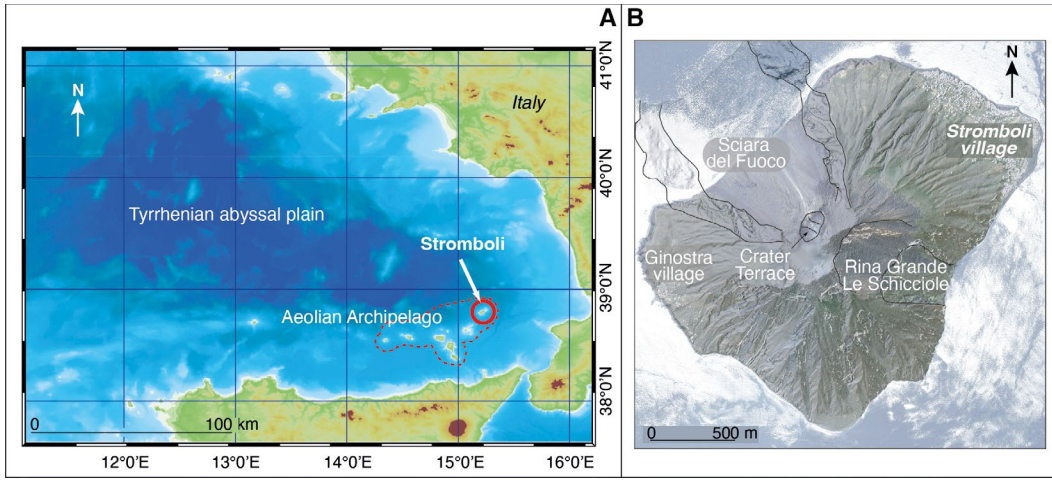

Fig. 1 **A** Location of Stromboli in the South Tyrrhenian Sea. **B** Orthophoto (PLEIADES-1) of the island of Stromboli, superimposed on a topo-bathymetric model, highlighting the primary geological-volcanological features and the two inhabited areas (modified from Di Traglia et al. 2023)

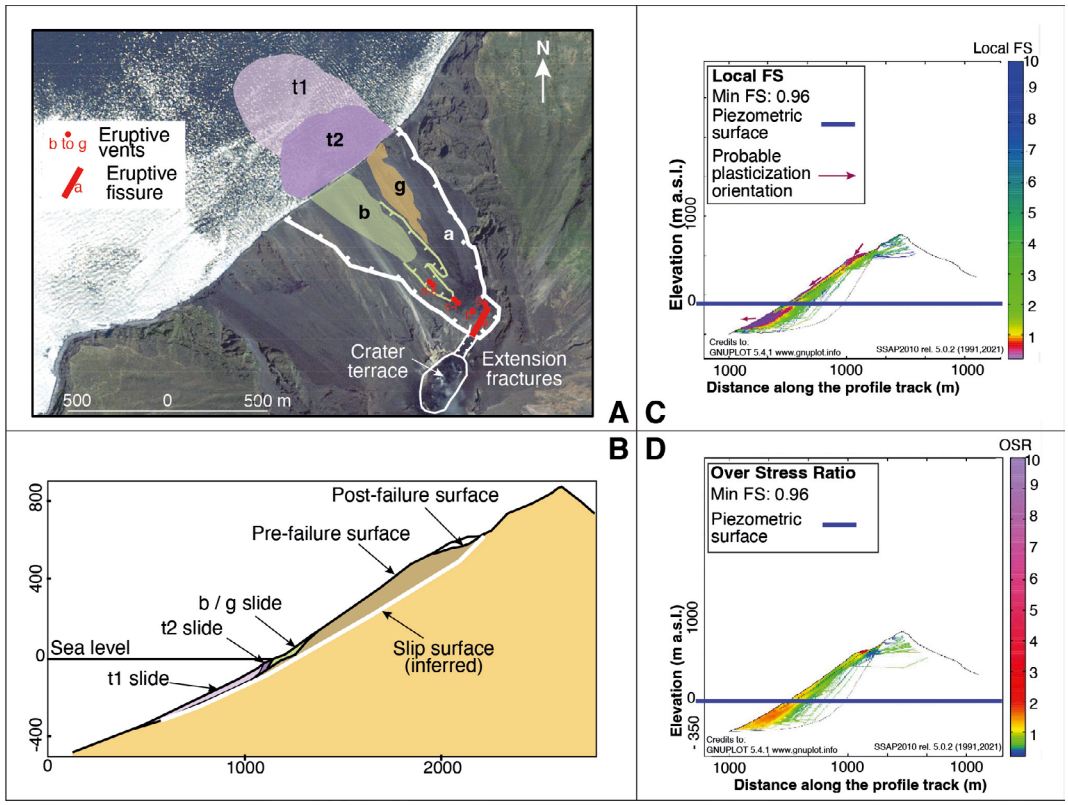

Fig. 2 **A** Map and **B** Schematic profile reconstructing the 2002 landslide sequence. The results of the back-analysis related to the 2002 landslide sequence are reported in **C** as a Factor of Safety profile and **D** Over Stress Ratio profile. Both profiles show the 2D stability results of the Sciara del Fuoco, accounting for the heterogeneity of the slope deposits, characterized by the irregular alternation of layers of volcaniclastic deposits and underlying lava levels (from Di Traglia et al. 2023)

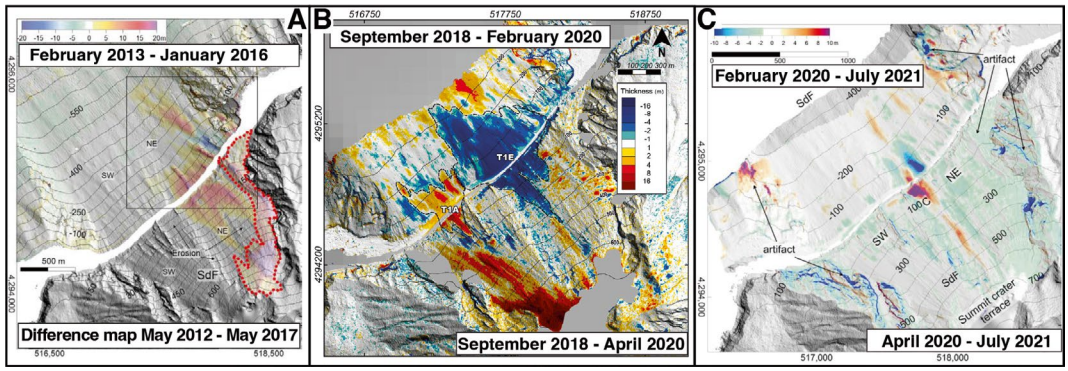

Fig. 3 Difference maps of the Sciara del Fuoco collapse scar (Stromboli), showing the main morphological changes induced by: **A** the 2014 effusive eruption (Casalbore et al. 2021), **B** the 2019 pyroclastic density currents and subsequent lava overflows (Di Traglia et al. 2022), and **C** the May 2021 pyroclastic density current due to crater rim failure and subsequent lava overflows (Casalbore et al. 2022). Dates in the upper and lower parts refer to the pre- and post-eruption topographic and bathymetric surveys, respectively

References

Barsotti S, Oddsson B, Gudmundsson MT, Pfeffer MA, Parks MM, Ófeigsson BG, Sigmundsson F, Reynisson,V, Jónsdóttir K, Roberts MJ, Heiðarsson EP, Jónasdóttir EB, Einarsson P, Jóhannsson T, Gylfason ÁG, Vogfjörd K (2022) Operational response and hazards assessment during the 2014–2015 volcanic crisis at Bárðarbunga volcano and associated eruption at Holuhraun, Iceland. J Volcanol Geoth Res 390:106753. https://doi.org/10.1016/j.jvolgeores.2019.106753

Björnsson H, Einarsson P (1990) Volcanoes beneath Vatnajökull, Iceland: evidence from radio echo-sounding, earthquakes and jökulhlaups. Jokull 40:147–168

Calvari S, Spampinato L, Lodato L, Harris AJL, Patrick MR, Dehn J, Burton MR, Andronico D (2005) Chronology and complex volcanic processes during the 2002–2003 flank eruption at Stromboli volcano (Italy) reconstructed from direct observations and surveys with a handheld thermal camera. J Geophys Res 110:B02201. https://doi.org/10.1029/2004JB003129

Calvari S, Nunnari G (2023) Statistical insights on the eruptive activity at Stromboli Volcano (Italy) recorded from 1879 to 2023. Rem Sens 15:4822. https://doi.org/10.3390/rs15194822

Carracedo JC, Troll VR (2016) The geology of the Canary Islands. Elsevier, ISBN 9780128096635

Carracedo JC, Troll VR, Day JMD, Geiger H, Aulinas M, Soler V, Deegan FM, Perez-Torrado FJ, Gisbert G, Gazel E, Rodriguez-Gonzalez A, Albert H (2022) The 2021 eruption of the Cumbre Vieja volcanic ridge on La Palma, Canary Islands. Geol Today 38:94–107. https://doi.org/10.1111/gto.12388

Carracedo JC, Troll VR (2021) North-East Atlantic Islands: The macaronesian archipelagos. In: Encyclopedia of Geology, vol 1–6, 2nd edn, vol 4: 674–699. Elsevier. https://doi.org/10.1016/B978-0-08-102908-4.00027-8

Casalbore D, Passeri F, Tommasi P, Verrucci L, Bosman A, Romagnoli C, Chiocci FL (2020) Small-scale slope instability on the submarine flanks of insular volcanoes: The case-study of the Sciara del Fuoco slope (Stromboli). Int J Earth Sci 109:2643–2658. https://doi.org/10.1007/s00531-020-01853-5

Casalbore D, Di Traglia F, Bosman A, Romagnoli C, Casagli N, Chiocci FL (2021) Submarine and subaerial morphological changes associated with the 2014 eruption at Stromboli Island. Rem Sens 13:2043. https://doi.org/10.3390/rs13112043

Casalbore D, Di Traglia F, Romagnoli C, Favalli M, Gracchi T, Tacconi Stefanelli C, Chiocci FL (2022) Integration of remote sensing and offshore geophysical data for monitoring the short-term morphological evolution of an active volcanic flank: a case study from Stromboli Island. Rem Sens 14(18):4605. https://doi.org/10.3390/rs14184605

Chiocci FL, Romagnoli C, Tommasi P, Bosman A (2008) The Stromboli 2002 tsunamigenic submarine slide: Characteristics and possible failure mechanisms. J Geophys Res, Solid Earth 113, B10102. htpps://doi.org/10.1029/2007JB005172

Di Traglia F et al (2018) Lava delta deformation as a proxy for submarine slope instability. Earth Planet Sci Lett 488:46–58. https://doi.org/10.1016/j.epsl.2018.01.038

Di Traglia F et al (2022) Subaerial-submarine morphological changes at Stromboli volcano (Italy) induced by the 2019–2020 eruptive activity. Geomorph 400:108093. https://doi.org/10.1016/j.geomorph.2021.108093

Di Traglia F et al (2023) Assessing flank instability of Stromboli volcano (Italy) by the reappraising of the 30 December 2002 tsunamigenic landslides. Landslides 20:1363–1380. https://doi.org/10.1007/s10346-023-02043-5

Gertisser R, Troll VR, Walter T, Nandaka IGMA, Ratdomopurbo A (2023). Merapi volcano: geology, eruptive activity, and monitoring of a high-risk volcano. Collection Active Volcanoes of the World. Springer Cham, pp XIX, 572. ISBN 978–3–031–15039–5.

Gisbert G, Troll VR, Day JMD, Geiger H, Perez-Torrado FJ, Aulinas M, Deegan FM, Albert H, Carracedo JC (2023) Reported ultra-low lava viscosities from the 2021 La Palma eruption are potentially biased. Nat Commun 14:6453. https://doi.org/10.1038/s41467-023-42022-x

Global Volcanism Program (2023). Merapi (263250). In: [Database] Volcanoes of the World (v. 5.1.4; 9 Nov 2023). Distributed by Smithsonian Institution, compiled by E. Venzke. https://doi.org/10.5479/si.GVP.VOTW5-2023.5.1

Gudmundsson MT, Jónsdóttir K, Hooper A, Holohan EP, Halldórsson SA, Ófeigsson BG, Cesca S, Vogfjörd KS, Sigmundsson F, Högnadóttir T, Einarsson P, Sigmarsson O, Jarosch AH, Jónasson K, Magnússon E, Hreinsdóttir S, Bagnardi M, Parks MM, Hjörleifsdóttir V, Pálsson F, Walter TR, Schöpfer MPJ, Heimann S, Reynolds HI, Dumont S, Bali E, Gudfinnsson GH, Dahm T, Roberts MJ, Hensch M, Belart JMC, Spaans K, Jakobsson S, Gudmundsson GB, Fridriksdóttir HM, Drouin V, Dürig T, Aðalgeirsdóttir G, Riishuus MS, Pedersen GBM, Boeckel T van, Oddsson B, Pfeffer MA, Barsotti S, Bergsson B, Donovan A, Burton MR, Aiuppa A (2016) Gradual caldera collapse at Bárdarbunga volcano, Iceland, regulated by lateral magma outflow. Science 353. https://doi.org/10.1126/science.aaf8988

Halldórsson SA, Bali E, Hartley ME, Neave DA, Peate DW, Guðfinnsson GH, Bindeman I, Whitehouse MJ, Riishuus MS, Pedersen GBM, Jakobsson S, Askew R, Gallagher CR, Guðmundsdóttir ER, Gudnason J, Moreland WM, Óskarsson BV, Nikkola P, Reynolds HI, Schmith J, Thordarson T (2018) Petrology and geochemistry of the 2014–2015 Holuhraun eruption,

central Iceland: compositional and mineralogical characteristics, temporal variability and magma storage. Contrib Mineral Petrol 173:64. https://doi.org/10.1007/s00410-018-1487-9

Hill H (1893) The volcanic outburst at Te Mari, Tongariro, in November, 1892. Trans NZ Inst 26:388–392

Hjartardóttir ÁR, Einarsson P, Gudmundsson MT, Högnadóttir T (2016) Fracture movements and graben subsidence during the 2014 Bárðarbunga dike intrusion in Iceland. J Volcanol Geoth Res 310:242–252. https://doi.org/10.1016/j.jvolgeores.2015.12.002

Hobden BJ (1997) Modelling magmatic trends in time and space: eruptive and magmatic history of Tongariro Volcanic complex, New Zealand. Unpublished PhD thesis, University of Canterbury

Jolly GE, Keys HJR, Procter JN, Deligne NI (2014b) Overview of the co-ordinated risk-based approach to science and management response and recovery for the 2012 eruptions of Tongariro volcano, New Zealand. J Volcanol Geoth Res 286:184–207. https://doi.org/10.1016/j.jvolgeores.2014.08.028

Jolly AD, Jousset P, Lyons JJ, Carniel R, Fournier N, Fry B, Miller C (2014a) Seismo-acoustic evidence for an avalanche driven phreatic eruption through a beheaded hydrothermal system: an example from the 2012 Tongariro eruption. J Volcanol Geotherm Res 286:331–347. https://doi.org/10.1016/j.jvolgeores.2014.04.007

Pedersen GBM, Höskuldsson A, Dürig T, Thordarson T, Jónsdóttir I, Riishuus MS, Óskarsson BV, Dumont S, Magnusson E, Gudmundsson MT, Sigmundsson F, Drouin VJPB, Gallagher C, Askew R, Gudnason J, Moreland WM, Nikkola P, Reynolds HI, Schmith J (2017) Lava field evolution and emplacement dynamics of the 2014–2015 basaltic fissure eruption at Holuhraun, Iceland. J Volcanol Geoth Res 340: 155–169. https://doi.org/10.1016/j.jvolgeores.2017.02.027

Procter J, Cronin SJ, Fuller IC, Lube G, Manville V (2010) Quantifying the geomorphic impacts of a lake-breakout lahar, Mount Ruapehu, New Zealand. Geology 38(1):67–70. https://doi.org/10.1130/G30129.1

Siebert L, Glicken H, Ui T (1987) Volcanic hazards from Bezymianny and Bandai-type eruptions. Bull Volcanol 49:435–459. https://doi.org/10.1007/BF01046635

Sigmundsson F, Hooper A, Hreinsdóttir S, Vogfjörd KS, Ófeigsson BG, Heimisson ER, Dumont S, Parks M, Spaans K, Gudmundsson GB, Drouin V, Árnadóttir T, Jónsdóttir K, Gudmundsson MT, Högnadóttir T, Fridriksdóttir HM, Hensch M, Einarsson P, Magnússon E, Samsonov S, Brandsdóttir B, White RS, Ágústsdóttir T, Greenfield T, Green RG, Hjartardóttir ÁR, Pedersen R, Bennett RA, Geirsson H, La Femina PC, Björnsson H, Pálsson F, Sturkell E, Bean CJ, Möllhoff M, Braiden AK, Eibl EPS (2015) Segmented lateral dyke growth in a rifting event at Bárðarbunga volcanic system, Iceland. Nature 517:191–195. https://doi.org/10.1038/nature14111

Troll VR, Aulinas M, Carracedo JC, Geiger H, Perez-Torrado FJ, Soler V, Deegan FM, Bloszies C, Weis F, Albert H, Gisbert G, Day JMD, Rodríguez-González A, Gazel E, Dayton K (2024) The 2021 La Palma eruption; social dilemmas resulting from living close to an active volcano. Geol Today 40(3):96–111. https://doi.org/10.1111/gto.12472

Yamamoto T, Nakamura Y, Glicken H (1999) Pyroclastic density current from the 1888 phreatic eruption of Bandai volcano, NE Japan. J Volcanol Geoth Res 90(3–4):191–207. https://doi.org/10.1016/S0377-0273(99)00025-6

Zemeny A, Zellmer GF, Ubide T, Smith IEM, Procter J, Tapu AT, Zernack AV (2023) Investigation of the Mid-Age (65–34 ka) Period of Taranaki Volcano, New Zealand: indications for the effect of volcano growth. J Petrol 64(5). https://doi.org/10.1093/petrology/egad027